Lattice Vibration Spectra. LX. Lattice Dynamical Calculations on Spinel Type MCr_2S_4 (M = Mn, Fe, Cd)

H. D. Lutz, J. Himmrich, and H. Haeuseler

Universität Siegen, Anorganische Chemie I, Siegen

Z. Naturforsch. **45a**, 893–902 (1990); received April 9, 1990

Lattice dynamical calculations of the spinel type MCr_2S_4 (M = Mn, Fe, Cd) have been done using various potential models (short-range, rigid-ion, polarizable-ion). The main results are that (i) the vibrational modes (eigenvectors) and potential energy distributions of the Raman and IR allowed phonon modes of the three chromium sulfides are very similar, (ii) the A-X and B-X short-range force constants (referring to AB_2X_4) strongly depend on the structural parameter u, i.e., the tetrahedral A-X force constants are smaller than the respective octahedral B-X ones opposite to previous calculations on the basis of an ideal spinel structure with $u = 0.25$, (iii) bending force constants (X-A-X and X-B-X), but not X-X and B-B repulsive forces, are negligible, (iv) in the case of the breathing mode of the tetrahedral AX_4 unit (species A_{1g}) the demand on B-X and X-X (stretching and repulsion) forces is larger than that on the A-X force, and (v) the effective dynamic charges of the bivalent metal ions are nearly zero.

Key words: Chromium sulfides, Spinels, Lattice dynamics, Force constant calculation, Vibrational modes.

1. Introduction

Among the ternary chalcogenides $A^{II}B_2^{III}X_4$, spinel type compounds are of considerable experimental and theoretical interest. Thus, magnetic and electric properties, structural features, such as structure maps and cation distributions with regard to the tetrahedral and octahedral sites, and vibrational behaviour in terms of bonding, ionicity, and free carrier contribution have been studied thoroughly in the last four decades.

In order to get more detailed information on bonding, structure, and dynamics of the spinel structure, lattice dynamical calculations should be a valuable tool. Such calculations, which are performed since the early seventies [1–8], are mostly based on relatively crude models and suffer from the lack of complete experimental IR and Raman data. Thus, apart from one rigid-ion model (RIM) calculation [5] (see also [9]) simple short-range models (SRM), e.g., valence force fields, were used until very recently [10]. Furthermore, most calculations were performed on the basis of the ideal spinel structure neglecting the structural parameter u of the real crystal structure.

Very recently single crystal Raman data [11] as well as the transversal and longitudinal optical zone centre phonon frequencies of the IR allowed modes [12, 13] became available for several chalcogenide spinels. Using these data, we carried out an improved treatment of the lattice dynamics of spinel type $A^{II}Cr_2S_4$ (A^{II} = Mn, Fe, Cd). In order to assess the physical meaning of the results obtained we employed several force field models, viz., an improved Shimanouchi SRM [14] as well as a RIM [15] and a polarizable-ion model (PIM) [16]. PIM calculations on spinels were performed for the first time. In the case of $MnCr_2S_4$ and $FeCr_2S_4$ no lattice dynamical calculations using IR and Raman data were yet reported.

The compounds under discussion are so-called normal spinels where A^{II} and chromium occupy only tetrahedral and octahedral sites, respectively. Lattice dynamical calculations on inverse spinels such as $A^{II}In_2S_4$ (A^{II} = Fe, etc.) are more complicated owing to the lack of full translational symmetry in these compounds (see the discussion given in [11]).

Reprint requests to Prof. Dr. H. D. Lutz, Anorganische Chemie I, Universität-Gesamthochschule, D-5900 Siegen.

2. Structure Data, Symmetry Coordinates, and Phonon Frequencies

Normal spinels AB_2X_4 crystallize in the space group $Fd\bar{3}m\text{-}O_h^7$. A part of the spinel structure is shown in Figure 1. The primitive rhombohedral unit cell contains two formula units. The fractional coordinates of the respective atoms given in Table 1 refer to

0932-0784 / 90 / 0700-0893 $ 01.30/0. – Please order a reprint rather than making your own copy.

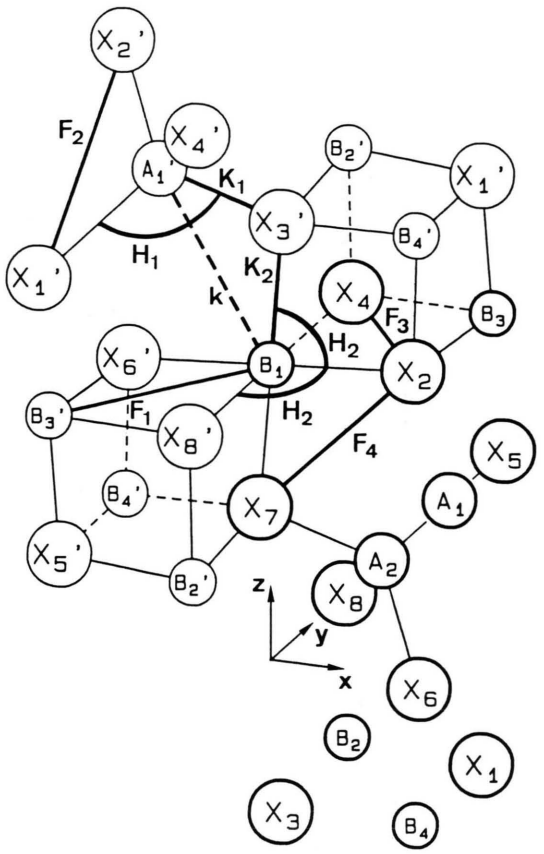

Fig. 1. Part of the spinel structure AB_2X_4 (marking of the atoms and short-range force constants see Tables 1 and 3, respectively).

Table 1. Lattice constants a and structural parameters u of spinel type MCr_2S_4 [17] and fractional coordinates of the 14 atoms in the primitive rhombohedral unit cell of spinels (see Figure 1).

Atom	x	y	z
A_1	3/8	7/8−1	3/8
A_2	1/8	1/8	1/8
B_1	0	0	1/2
B_2	0	1/4	3/4−1
B_3	1/4	1/4	1/2
B_4	1/4	0	3/4−1
X_1	$-u+1/2$	$-u+1/2$	$-u$
X_2	$-u+1/2$	$u+3/4-1$	$u+1/4$
X_3	$u+3/4-1$	$u+3/4-1$	$-u$
X_4	$u+3/4-1$	$-u+1/2$	$u+1/4$
X_5	u	u	u
X_6	u	$-u+1/4$	$-u+1/4$
X_7	$-u+1/4$	$-u+1/4$	u
X_8	$-u+1/4$	u	$-u+1/4$

$MnCr_2S_4$: $a=1010.70$ pm, $u=0.2620$; $FeCr_2S_4$: $a=998.93$ pm, $u=0.2595$; $CdCr_2S_4$: $a=1023.9$ pm, $u=0.2650$.

the cubic system (x, y, z). The lattice constants a and the structural parameters u of the spinels under discussion were taken from Hill et al. [17] (see Table 1).

Group theoretical treatment of the optical zone centre ($|\boldsymbol{k}|=0$) phonon modes [18] yields

$$\Gamma = A_{1g} + E_g + F_{1g} + 3F_{2g} + 2A_{2u} + 2E_u + 4F_{1u} + 2F_{2u}.$$

There are five Raman-active (A_{1g}, E_g, $3F_{2g}$) and four IR-active modes ($4F_{1u}$). The symmetry coordinates of the Raman and IR allowed modes [18] are listed in Table 2. The band frequencies used for the calculations reported in this work were taken from the literature (see [11–13, 19] and further references cited therein) (see Table 4).

3. Potential Model

The lattice dynamical calculations were carried out according to the Wilson-GF-matrix method on the basis of cartesian symmetry coordinates [2, 14]. The potential model used is as described in the literature [20, 21]. For details see also [19]. It is built up in three stages. The first part is a short-range valence force model (SRM). In the second part this model is extended to a RIM by addition of Coulomb forces. The third part results in the PIM where the polarizabilities of the ions are also taken into account. According to Yamamoto et al. [20], the dynamical matrix $\mathbf{D}$ is given by

$$\mathbf{D} = \bar{\mathbf{M}}(\mathbf{F}^N + \mathbf{F}^C + \mathbf{F}^I + \mathbf{F}^M)\bar{\mathbf{M}},$$

where $\bar{\mathbf{M}}$ is a diagonal matrix specifying the masses $m_k^{-1/2}$ of the atoms involved.

The matrix $\mathbf{F}^N$ represents the non-Coulombic short-range interactions with valence and repulsive force constants K_i and F_i, bending force constants H_i, and interaction force constants k_i [1, 2, 5]. The Coulomb matrix $\mathbf{F}^C$ is given by the expression

$$\mathbf{F}^C = \mathbf{Z}\bar{\mathbf{Q}}\mathbf{Z}.$$

In this equation, $\mathbf{Z}$ is a diagonal matrix specifying the effective dynamical charges z_k and $\bar{\mathbf{Q}}$ is a matrix derived from the Coulomb coefficient matrix $\mathbf{Q}$. $\mathbf{Q}$, which is calculated by Ewald's method, represents the electrostatic interactions of the ions present. If electronic polarizability is taken into account, an additional Coulomb interaction matrix $\mathbf{F}^I$ due to induced

Table 2. Symmetry coordinates of the Raman and IR allowed modes in terms of Cartesian coordinates x, y, z (for the silent modes see [18]). In the case of the double and triple degenerate species the coordinates q_b and q_a of [18] are given.

Species	Nr.	x	y	z	x	y	z	x	y	z	x	y	z
		A_1			A_2								
F_{2g}	q_3	c	0	0	$-c$	0	0						
F_{1u}	q_6	c	0	0	c	0	0						
		B_1			B_2			B_3			B_4		
F_{1u}	q_7	e	0	0	e	0	0	e	0	0	e	0	0
F_{1u}	q_8	0	d	d	0	$-d$	$-d$	0	d	$-d$	0	$-d$	d
		X_1			X_2			X_3			X_4		
A_{1g}	q_1	a	a	a	a	$-a$	$-a$	$-a$	$-a$	a	$-a$	a	$-a$
E_g	q_2	0	b	$-b$	0	$-b$	b	0	$-b$	$-b$	0	b	b
F_{2g}	q_4	d	0	0	d	0	0	d	0	0	d	0	0
F_{2g}	q_5	0	b	b	0	$-b$	$-b$	0	b	$-b$	0	$-b$	b
F_{1u}	q_9	d	0	0	d	0	0	d	0	0	d	0	0
F_{1u}	q_{10}	0	b	b	0	$-b$	$-b$	0	b	$-b$	0	$-b$	b
		X_5			X_6			X_7			X_8		
A_{1g}	q_1	$-a$	$-a$	$-a$	$-a$	a	a	a	a	$-a$	a	$-a$	a
E_g	q_2	0	$-b$	b	0	b	$-b$	0	b	b	0	$-b$	$-b$
F_{2g}	q_4	$-d$	0	0	$-d$	0	0	$-d$	0	0	$-d$	0	0
F_{2g}	q_5	0	$-b$	$-b$	0	b	b	0	$-b$	b	0	b	$-b$
F_{1u}	q_9	d	0	0	d	0	0	d	0	0	d	0	0
F_{1u}	q_{10}	0	b	b	0	$-b$	$-b$	0	b	$-b$	0	$-b$	b

$a=1/\sqrt{24}$; $b=1/4$; $c=1/\sqrt{2}$; $d=1/\sqrt{8}$; $e=1/2$.

Force constant[a]	Internal coordinate	No.[b]	Interatomic distances (pm) and angles (°)[c]		
			$MnCr_2S_4$	$FeCr_2S_4$	$CdCr_2S_4$
K_1 (f_1)	A-X	8	239.83	232.71	248.28
K_2 (f_2)	B-X	24	241.16	240.62	241.59
k (f_4)	AX-BX[d]	24	419.01[e]	414.13[e]	424.49[e]
F_1 (f_3)	B-B	12	357.34	353.18	362.00
H_1 (f_5)	X-A-X	12	109.471	109.471	109.471
H_2 (f_6)	X-B-X	24	84.096	85.394	82.492
		24	95.904	94.606	97.508
F_2	X-X	12	391.64	380.02	405.44
F_3	X-X	12	323.03	326.33	318.56
F_4	X-X	24	358.16	353.68	363.30

Table 3. Short-range force constants and respective interatomic distances.

[a] Labelling of the short-range force constants given in parentheses correspond to those reported in [2].
[b] Number of internal coordinates per primitive unit cell.
[c] Calculated from literature data [17] of a and u (see Table 1).
[d] Off-diagonal force constant representing the interaction between the tetrahedral and octahedral unit of the structure.
[e] Distance A-B.

dipole interactions must be added,

$$\mathbf{F}^{I} = -\mathbf{Z}\bar{\mathbf{Q}}(\mathbf{A}^{-1} - \mathbf{Q})^{-1}\bar{\mathbf{Q}}\mathbf{Z},$$

where **A** is a diagonal matrix containing the elements of the polarizability tensor. The matrix $\mathbf{F}^{M}$ is the macroscopic field matrix describing the TO/LO splitting of the phonon modes.

For mathematical reasons the maximum number of force field parameters which can be determined from a lattice dynamical calculation is given by the number of observed vibrational frequencies, which is ten (or fifteen, comprising the LO phonons) in the case of spinels if the translation T is included.Therefore, the number of short-range valence force constants is limited to ten. In our calculation, we used six valence and repulsive force constants K_1, K_2, F_1, F_2, F_3, F_4, two bending force constants H_1, H_2, and one interaction force constant k (see Table 3). In addition to these

Table 4. Observed [11, 12, 19] (FRQ) and calculated (FRC) phonon frequencies (cm^{-1}).

Species		$MnCr_2S_4$				$FeCr_2S_4$				$CdCr_2S_4$			
		FRQ	FRC			FRQ	FRC			FRQ	FRC		
			SRM	RIM	PIM		SRM	RIM	PIM		SRM	RIM	PIM
A_{1g}		378	379	379	378	377	379	379	377	391	390	388	389
E_g		251	247	251	256	251	247	247	254	254	256	260	257
F_{2g} (1)		346	348	348	347	344	348	350	346	346	347	347	347
F_{2g} (2)		282	277	277	278	284	275	274	277	279	278	278	278
F_{2g} (3)			109	108	108		106	105	106	96	84	82	83
F_{1u} (1)	TO	381	385	391	388	382	388	392	390	380	380	384	383
F_{1u} (2)		322	322	322	322	321	321	320	319	324	324	326	323
F_{1u} (3)		262	257	258	260	265	257	262	264	240	240	241	241
F_{1u} (4)		121	128	126	125	114	124	122	122	95	107	104	103
F_{1u} (1)	LO	397		391	389	396		392	390	392		385	388
F_{1u} (2)		342		342	344	341		340	344	348		348	350
F_{1u} (3)		263		259	260	267		263	264	242		242	241
F_{1u} (4)		122		126	125	118		122	123	98		104	103
Figure of merit[a]			3.9	4.1	3.7		5.8	5.3	4.5		5.4	5.3	4.7

[a] Calculation $f = \sqrt{\left(\sum_{i=1}^{N} (\mathrm{FRQ(I)} - \mathrm{FRC(I)})^2 / N\right)}$.

Table 5. Short range force constants (N/cm), effective dynamical charges (e), and electronic polarizabilities (10^6 pm^3).

Force constant	Internal coordinate	$MnCr_2S_4$			$FeCr_2S_4$			$CdCr_2S_4$			
		SRM	RIM	PIM	SRM	RIM	PIM	SRM	RIM	PIM	[5]
K_1	A-X	0.45	0.43	0.42	0.41	0.40	0.40	0.56	0.52	0.50	1.00
K_2	B-X	0.68	0.78	0.85	0.68	0.75	0.87	0.72	0.85	0.90	1.00
k	AX-BX	0.00	0.00	0.00	0.00	0.00	0.00	0.00	0.00	0.00	
F_1	B-B	0.45	0.45	0.51	0.48	0.50	0.60	0.29	0.27	0.32	
F_2	X-X	0.10	0.10	0.10	0.10	0.10	0.10	0.12	0.11	0.11	
F_3	X-X	0.24	0.24	0.24	0.24	0.24	0.24	0.26	0.25	0.25	0.08
F_4	X-X	0.14	0.13	0.12	0.14	0.14	0.12	0.12	0.11	0.09	
H_1	X-A-X	0.00	0.00	0.00	0.00	0.00	0.00	0.00	0.00	0.00	0.00
H_2	X-B-X	0.04	0.02	0.02	0.04	0.03	0.02	0.03	0.01	0.02	0.00
z_A			0.00	0.00		0.00	0.00		0.00	0.00	0.65
z_B			0.72	0.72		0.72	0.72		0.80	0.80	0.70
z_X			−0.36	−0.36		−0.36	−0.36		−0.40	−0.40	−0.51
z_X[a]				−0.51			−0.45			−0.51	
α_A				1.5			1.5			0.2	
α_B				1.4			1.4			0.0	
α_X				3.5			3.8			5.3	
ε_∞				5.6			7.1			7.1	
ε_∞[b]				5.9			8.3			6.9	

[a] Szigeti charge obtained from the TO/LO splittings [12].
[b] High frequency dielectric constant obtained by classical oscillator-fit calculation [12].

short-range parameters, two effective dynamical charges (the third one is given by the electroneutrality condition) have to be added in the RIM, and moreover three polarizabilities in the PIM.

The lattice dynamical calculations were carried out on a DIGITAL VAX 8820 system and an IBM-PC/AT compatible computer. For a detailed description of the self-made program see [19]. The input parameters are the fractional coordinates (x, y, z), the unit cell dimensions a, the structural parameters u, the masses of the atoms m_k, the symmetry coordinates q_n, and the phonon frequencies ω_j. The short-range valence

Table 6. Eigenvectors of the Raman and IR allowed phonon modes with respect to the symmetry coordinates $q_1 - q_5$ and $q_6 - q_{10}$ given in Table 2 obtained by polarizable-ion model (PIM) calculations.

Compound	Species	q_1	q_2	q_3	q_4	q_5
$MnCr_2S_4$	A_{1g}	1.000				
	E_g		1.000			
	F_{2g} (1)			−0.100	−0.386	0.917
	F_{2g} (2)			−0.262	0.899	0.350
	F_{2g} (3)			0.960	0.205	0.191
$FeCr_2S_4$	A_{1g}	1.000				
	E_g		1.000			
	F_{2g} (1)			−0.092	−0.395	0.914
	F_{2g} (2)			−0.249	0.898	0.363
	F_{2g} (3)			0.964	0.194	0.181
$CdCr_2S_4$	A_{1g}	1.000				
	E_g		1.000			
	F_{2g} (1)			−0.091	−0.280	0.956
	F_{2g} (2)			−0.184	0.948	0.261
	F_{2g} (3)			0.979	0.153	0.138

Compound	Species	q_6	q_7	q_8	q_9	q_{10}
$MnCr_2S_4$	F_{1u} (1) TO	−0.070	0.037	0.814	0.012	0.575
	LO	−0.065	0.084	0.814	−0.033	0.570
	F_{1u} (2) TO	0.116	0.690	0.084	−0.697	−0.134
	LO	0.098	0.700	0.001	−0.695	−0.133
	F_{1u} (3) TO	−0.233	0.214	−0.566	−0.041	0.760
	LO	−0.241	0.178	−0.572	−0.002	0.764
	F_{1u} (4) TO	0.858	−0.339	−0.099	−0.257	0.271
	LO	0.858	−0.331	−0.099	−0.264	0.273
$FeCr_2S_4$	F_{1u} (1) TO	−0.059	0.026	0.849	0.016	0.524
	LO	−0.060	0.016	0.848	0.025	0.525
	F_{1u} (2) TO	0.112	0.690	0.089	−0.695	−0.144
	LO	0.085	0.708	0.066	−0.693	−0.085
	F_{1u} (3) TO	−0.216	0.216	−0.515	−0.052	0.800
	LO	−0.226	0.169	−0.519	−0.004	0.807
	F_{1u} (4) TO	0.862	−0.341	−0.082	−0.262	0.255
	LO	0.863	−0.331	−0.083	−0.272	0.256
$CdCr_2S_4$	F_{1u} (1) TO	−0.072	0.024	0.694	0.046	0.714
	LO	−0.055	0.201	0.688	−0.129	0.683
	F_{1u} (2) TO	0.077	0.700	0.086	−0.703	−0.055
	LO	0.083	0.678	−0.102	−0.688	−0.221
	F_{1u} (3) TO	−0.188	0.177	−0.706	0.017	0.660
	LO	−0.190	0.163	−0.709	0.031	0.658
	F_{1u} (4) TO	0.792	−0.420	−0.113	−0.363	0.227
	LO	0.792	−0.414	−0.112	−0.369	0.229

forces (K_i, H_i, F_i, k_i), the effective dynamical charges z_k, and the polarizabilities α_k are treated as variable parameters to give the best fit of the experimental frequencies.

4. Results

The observed and calculated frequencies are given in Table 4. The force field parameters (short-range force constants, effective dynamical charges, and polarizabilities) are listed in Table 5. The eigenvectors and potential energy distributions (PED) are given in Tables 6 and 7. The phonon frequencies and the PEDs of the silent modes (species A_{2u}, E_u, F_{1g}, F_{2u}), calculated with the force field parameters, are given in Tables 8 and 9. The vibrational modes of the zone-centre phonons obtained for $MnCr_2S_4$ calculated with the PIM are shown in Figs. 2 and 3, respectively. The vibrational modes of $FeCr_2S_4$ and $CdCr_2S_4$ are similar.

As main results of the lattice dynamical calculations the following points are emphasized:

(i) The sequence of the short-range stretching force constants K_1 (tetrahedron) and K_2 (octahedron) is reversed (i.e. $K_2 > K_1$) compared to the results reported in the literature [1, 2, 8].

(ii) The bending force constants H_1 and H_2 are negligible, but not the repulsive force constants F_1, F_2, F_3, and F_4.

(iii) The effective dynamic charges of the bivalent metals on the tetrahedral sites are nearly zero, those of the sulfide ions resemble the Szigeti charges obtained from the TO/LO splittings [12] fairly well (see Table 5).

(iv) The lacking Raman bands (species F_{2g}) of $MnCr_2S_4$ and $FeCr_2S_4$ are at about 108 and 106 cm^{-1}, respectively (see Table 4).

(v) The eigenvectors and PEDs of the respective TO and LO phonon modes differ only slightly (see Tables 6 and 7 and Figure 2).

(vi) The respective phonon modes of the various chromium sulfide spinels under investigation are very similar with respect to both eigenvectors (see Table 6) and PEDs (see Table 7).

(vii) The contributions of the A-X (K_1) and B-X (K_2) force constants to the potential energy of the IR active vibrations (see Table 7) as well as the motions of the various atoms in the vibrational modes (see Fig. 2) largely resemble the findings of the spectroscopic studies of both the isostructural series $A^{II}B_2^{III}S_4$ [11, 12] and sulfide spinel solid solutions [23], viz., contribution of K_1: $F_{1u}(4) \gg F_{1u}(3) > F_{1u}(2) > F_{1u}(1)$, K_2: $F_{1u}(2) > F_{1u}(1) \gg F_{1u}(3) \sim F_{1u}(4)$, motion of A: $F_{1u}(4) \gg F_{1u}(3) > F_{1u}(2) \sim F_{1u}(1)$, B: $F_{1u}(1) \sim F_{1u}(2) \sim F_{1u}(3) \gg F_{1u}(4)$, and X: $F_{1u}(1) \sim F_{1u}(2) \sim F_{1u}(3) \gg F_{1u}(4)$.

(viii) In opposition to conclusions from simple Raman studies [11] the PED of the total symmetric Ra-

Table 7. Potential energy distributions (%) of the Raman and IR allowed phonon modes.

Species	Force constant	Co-ordinate	$MnCr_2S_4$				$FeCr_2S_4$				$CdCr_2S_4$			
			SRM	RIM	PIM		SRM	RIM	PIM		SRM	RIM	PIM	
A_{1g}	F_3	X-X	36	35	35		36	35	35		36	35	35	
	K_2	B-X	20	23	25		21	23	27		19	22	24	
	K_1	A-X	17	16	15		15	15	15		20	18	18	
	F_2	X-X	15	14	15		15	15	15		16	15	15	
E_g	K_2	B-X	64	72	76		64	70	77		66	74	80	
	F_3	X-X	21	20	19		21	20	19		21	19	20	
	F_2	X-X	9	8	8		9	9	8		9	8	9	
	C	LRFC	–	−4	−7		–	−4	−7		–	−4	−12	
F_{2g} (1)	K_2	B-X	30	34	38		30	33	39		31	37	38	
	F_4	X-X	26	24	22		27	26	23		20	18	15	
	F_3	X-X	18	17	18		18	17	18		20	20	20	
	F_2	X-X	7	7	7		7	7	7		9	8	9	
F_{2g} (2)	K_2	B-X	38	44	49		40	45	51		43	50	54	
	K_1	A-X	34	33	31		32	31	29		31	29	26	
	F_4	X-X	16	15	14		16	14	14		19	16	15	
	F_3	X-X	4	4	4		5	5	4		2	3	3	
F_{2g} (3)	K_1	A-X	58	60	62		62	64	64		58	62	64	
	K_2	B-X	23	25	25		22	22	25		23	24	23	
	F_3	X-X	9	8	8		8	8	7		10	8	7	
	F_2	X-X	4	3	3		4	3	3		4	4	3	
F_{1u} (1)	K_2	B-X	56	62	(63)	67	(68)	55	58	(58)	67	(66)	63	72	(74)	71	(76)
TO (LO)	F_1	B-B	25	25	(25)	29	(29)	27	29	(29)	37	(37)	13	12	(12)	14	(13)
	C	LRFC	–	−2	(−2)	−12	(−12)	–	−2	(−2)	−17	(−17)	–	−4	(−4)	−10	(−9)
	F_3	X-X	6	6	(5)	6	(5)	6	5	(5)	5	(5)	9	8	(8)	9	(8)
F_{1u} (2)	K_2	B-X	70	81	(73)	93	(81)	73	81	(73)	96	(85)	72	85	(73)	101	(78)
TO (LO)	C	LRFC	–	−4	(8)	−12	(3)	–	−4	(8)	−14	(2)	–	−4	(9)	−17	(3)
	H_2	X-B-X	17	11	(9)	10	(9)	16	13	(11)	9	(8)	12	6	(5)	10	(9)
	K_1	A-X	12	10	(8)	8	(7)	9	9	(7)	8	(5)	13	11	(19)	6	(9)
F_{1u} (3)	F_1	B-B	32	29	(29)	31	(32)	32	28	(28)	30	(30)	34	29	(29)	36	(36)
TO (LO)	F_3	X-X	20	21	(21)	22	(22)	21	22	(22)	23	(23)	18	20	(20)	20	(20)
	K_1	A-X	20	21	(23)	21	(23)	19	19	(20)	20	(22)	18	19	(21)	20	(21)
	F_2	X-X	8	8	(8)	9	(9)	9	9	(9)	10	(10)	8	8	(9)	9	(8)
F_{1u} (4)	K_1	A-X	64	65	(65)	66	(67)	68	70	(70)	69	(69)	62	64	(65)	66	(66)
TO (LO)	F_3	X-X	13	12	(13)	12	(12)	12	10	(10)	11	(11)	15	14	(14)	13	(13)
	K_2	B-X	7	8	(7)	9	(8)	7	8	(7)	10	(9)	6	7	(6)	6	(5)
	F_2	X-X	5	5	(5)	5	(5)	5	4	(4)	5	(5)	7	6	(6)	6	(6)

Table 8. Phonon energies (cm^{-1}) of the silent modes.

Species	$MnCr_2S_4$			$FeCr_2S_4$			$CdCr_2S_4$			
	SRM	RIM	PIM	SRM	RIM	PIM	SRM	RIM	PIM	[1]
A_{2u} (1)	441	453	466	448	462	488	422	427	437	387
A_{2u} (2)	346	351	344	347	355	347	331	340	326	194
E_u (1)	358	359	350	360	358	353	357	358	357	323
E_u (2)	243	246	215	247	257	219	214	219	188	124
F_{1g}	240	242	244	239	240	243	241	244	233	216
F_{2u} (1)	322	322	310	324	320	308	323	324	311	322
F_{2u} (2)	146	136	115	147	142	107	132	122	103	68

Table 9. Potential energy distributions (%) of the silent modes.

Species	Force constant	Co-ordinate	$MnCr_2S_4$			$FeCr_2S_4$			$CdCr_2S_4$		
			SRM	RIM	PIM	SRM	RIM	PIM	SRM	RIM	PIM
$A_{2u}(1)$	F_1	B-B	48	48	50	52	54	57	21	22	24
	K_2	B-X	41	43	46	39	38	41	48	56	56
	F_3	X-X	5	4	4	4	2	3	15	13	13
	C	LRFC	–	1	−4	–	2	−4	–	−2	−4
$A_{2u}(2)$	F_3	X-X	34	35	35	35	35	36	24	26	27
	F_1	B-B	19	14	20	18	11	17	36	26	36
	K_1	A-X	16	16	15	15	15	15	13	13	14
	F_2	X-X	14	14	15	15	15	15	11	11	12
$E_u(1)$	K_2	B-X	58	66	73	59	65	74	62	72	75
	F_4	X-X	25	23	24	24	24	24	22	20	18
	C	LRFC	–	−6	−15	–	−6	−17	–	−7	−9
	F_3	X-X	7	7	8	7	7	8	8	8	8
$E_u(2)$	F_1	B-B	36	34	57	36	35	63	31	27	46
	C	LRFC	–	14	−23	–	13	−26	–	21	−27
	K_2	B-X	7	8	21	6	7	19	10	12	23
	H_2	X-B-X	28	17	20	27	19	17	26	12	27
F_{1g}	K_2	B-X	68	77	84	68	75	84	74	84	98
	F_4	X-X	26	23	21	26	25	22	22	19	18
	C	LRFC	–	−4	−8	–	−4	−8	–	−5	−20
	H_2	X-B-X	6	4	4	6	5	3	4	2	4
$F_{2u}(1)$	K_2	B-X	74	85	98	74	83	100	79	92	103
	C	LRFC	–	−7	−22	–	−7	−24	–	−9	−22
	F_4	X-X	19	18	19	19	19	20	16	14	15
	H_2	X-B-X	7	5	5	7	6	4	5	2	4
$F_{2u}(2)$	F_4	X-X	47	50	53	48	47	60	52	55	55
	K_2	B-X	10	14	40	10	15	57	9	13	42
	C	LRFC	–	5	−35	–	3	−59	–	10	−50
	H_2	X-B-X	43	31	42	41	35	42	39	22	53

man mode (species A_{1g}) exhibits larger contributions of B-X stretching (K_2) and X-X repulsive force constants (F_2 and F_3) than of the A-X stretching force constant (K_1). Further relations are K_1: $F_{2g}(3) > F_{2g}(2) \gg F_{2g}(1) \sim E_g$, K_2: $E_g > F_{2g}(1) \sim F_{2g}(2) > F_{2g}(3)$, motion of A: $F_{2g}(3) \gg F_{2g}(2) > F_{2g}(1)$, X: $F_{2g}(1) \sim F_{2g}(2) \gg F_{2g}(3)$.

(ix) The contributions of Coulomb forces (LRFC) are negligible except for the Raman allowed E_g band and the two highest-energy F_{1u} modes (see Table 7). For the IR active F_{1u} modes this corresponds to the large TO/LO splittings of these bands.

(x) Opposite to the short-range force constants, which strongly depend on the potential model used (see Table 5), the eigenvectors (vibrational modes) of the various phonon modes differ only slightly and resemble nicely those obtained by more crude potential models [1, 2] and even those proposed from symmetry considerations and spectroscopic studies of various spinel type compounds [18, 22].

5. Discussion

The short-range force constants obtained (see Table 5) reveal that (apart from Coulomb forces) the potential of the spinel structure, at least for chromium sulfides, is mainly controlled by B-X (K_2 octahedron) and A-X (K_1 tetrahedron) stretching as well as X-X (F_2–F_4) (see also [5]) and (surprisingly) B-B (F_1) repulsive forces, whereas bending forces (H_1, H_2) can be neglected. Thus, with the exception of $F_{1u}(2)$, X-X repulsive forces are important for all modes and B-B interactions are predominant for $F_{1u}(3)$ (and $F_{1u}(1)$) (see Table 7). The reason for the great importance of the Coulomb forces for $F_{1u}(2)$ (and to a smaller extend for E_g and $F_{1u}(1)$, see Table 7) is not clear so far.

Model calculations showed that the quantities of K_1 and K_2 are very sensitive to the A-X and B-X distances. Thus, the reversed order of these force constants compared to the literature data [1, 2, 4, 8] is owing to the use of the real bond distances in this

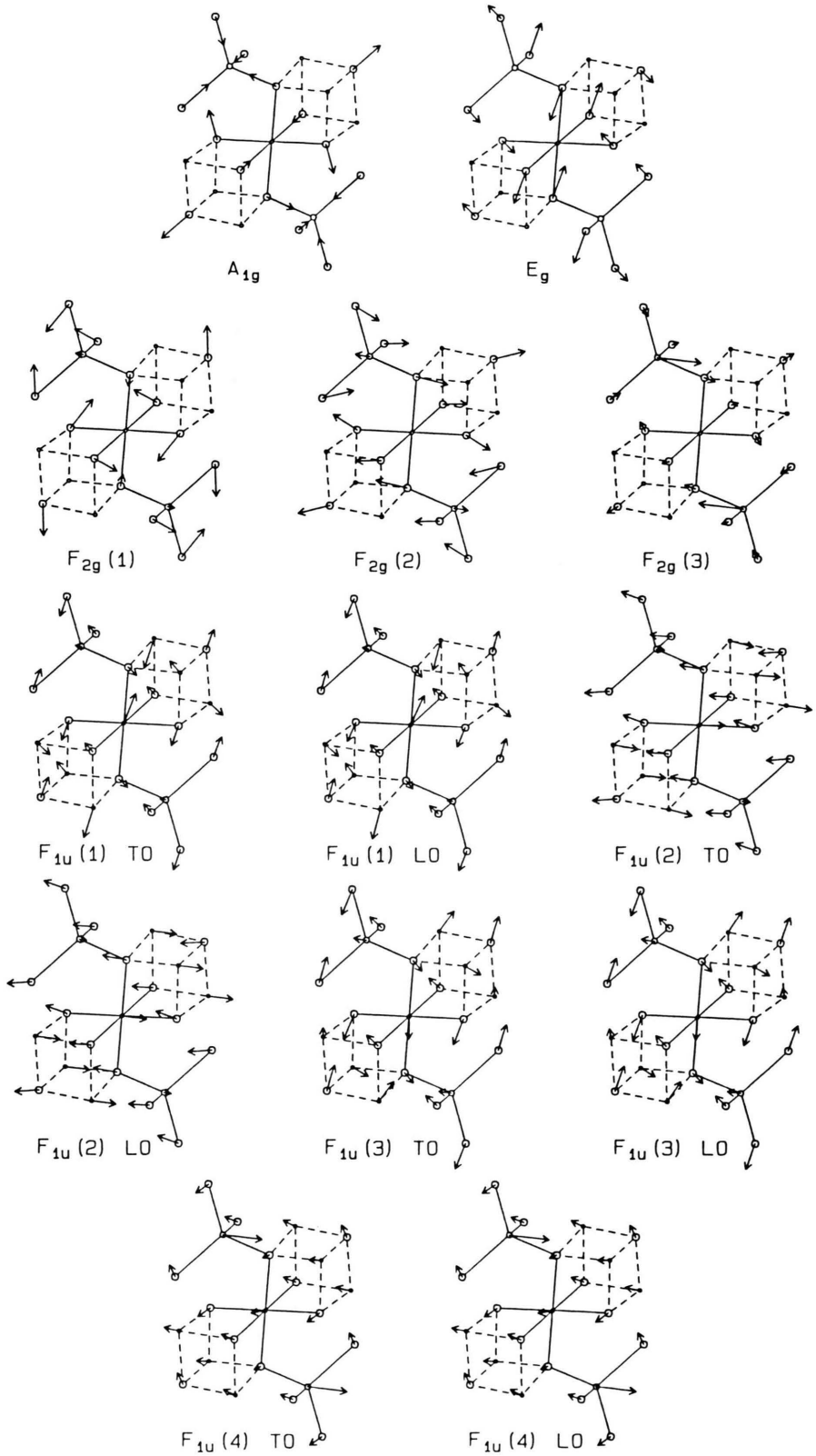

Fig. 2. Vibrational modes of the Raman and IR allowed zone centre phonons of $MnCr_2S_4$ obtained by polarizable-ion model (PIM) calculations.

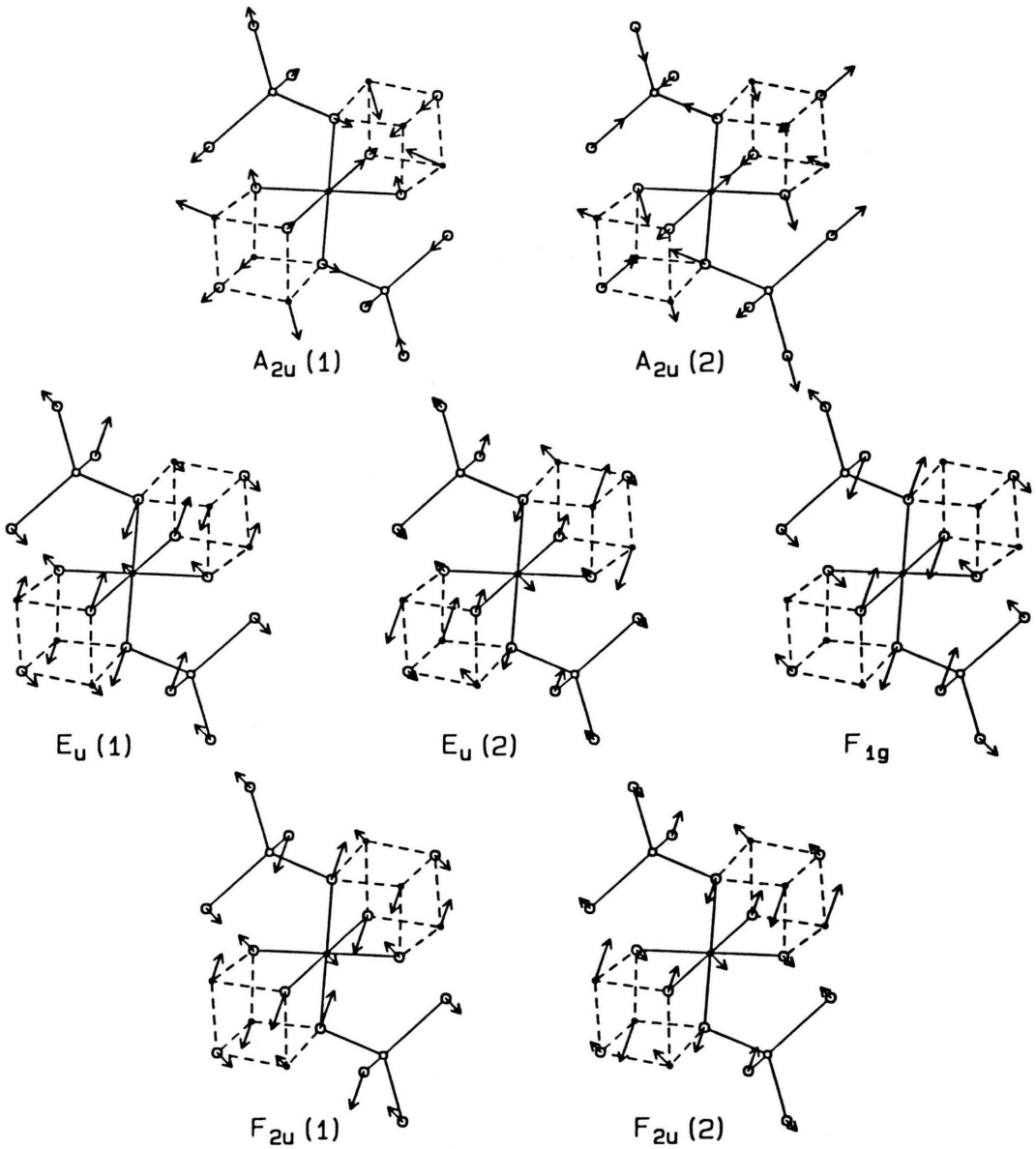

Fig. 3. Vibrational modes of the silent zone centre phonons of $MnCr_2S_4$ calculated from the obtained force field parameters (polarizable-ion model calculations).

work and, hence, is undoubtedly significant. The larger values of K_1 (compared to K_2) in previous works are obviously pretended by the wrong distances of the ideal (structural parameter $u=0.25$) spinel structure used.

From the dynamic effective charges obtained the nearly zero charge of the metal ions on the tetrahedral sites is remarkable. The question arises, how far these results give evidence for the static effective charge of the tetrahedrally coordinated metal ions in spinels. The polarizabilities obtained are reasonable with respect to the literature data (see, e.g. [24] and further references cited therein).

The vibrational modes of the zone centre phonons obtained (see Fig. 2) reveal that division into vibrations of the tetrahedral AX_4 and the octahedral BX_6

(or the cube B_4X_4) units of the structure proposed in the older literature (see, for instance [25]) is not possible. Instead of this, all modes must be regarded as coupled vibrations of these structural units. Thus, $F_{2g}(1)$ can be described as a "combination" of $\delta_{as}(\nu_4)$ of a tetrahedral AX_4 and $\delta(\nu_5)$ of an octahedral BX_6 unit, and $F_{1u}(2)$ as a "combination" of $\nu_{as}(\nu_3)$ of a tetrahedral AX_4 and one of the two F_{2g} modes of a cube-shaped B_4X_4 unit.

The energies calculated for the silent modes (and the respective potential energy distributions) differ somewhat with respect to the potential model used, especially in the case of $E_u(2)$ and $F_{2u}(2)$ (see Tables 8 and 9). The vibrational modes (and eigenvectors) obtained, however, are largely independent of the model used and, hence, are near to the true ones. The lattice vibration with the highest energy is $A_{2u}(1)$, which can be described as coupled antiphase breathing vibrations of both the AX_4 tetrahedra and the B_4X_4 cubes (see Figure 3).

[1] P. Brüesch and F. D'Ambrogio, Phys. Stat. Sol. B **50,** 513 (1972).
[2] H. D. Lutz and H. Haeuseler, Ber. Bunsenges. Phys. Chem. **79,** 604 (1975).
[3] H. Shimizu, Y. Ohbayashi, K. Yamamoto, and K. Abe, J. Phys. Soc. Jpn. **38,** 750 (1975).
[4] S. I. Boldish and W. B. White, Rare Earths Mod. Sci. Technol., 13th, 607 (1978), C.A. **91,** 219780.
[5] H. A. Lauwers and M. A. Herman, J. Phys. Chem. Solids **41,** 223 (1980).
[6] M. A. Aldzhanov, A. M. Aliev, R. K. Veliev, K. K. Mamedov, M. I. Mekhtiev, and V. Ya. Shteinshraiber, Phys. Stat. Sol. B **115,** K 75 (1983).
[7] M. Wakaki, Jpn. J. Appl. Phys., Part 1, **24,** 1471 (1985).
[8] K. Wakamura, H. Iwatani, and K. Takarabe, J. Phys. Chem. Solids **48,** 857 (1987).
[9] M. E. Striefler, and G. R. Barsch, J. Phys. Chem. Solids **33,** 2229 (1972).
[10] H. C. Gupta, G. Sood, A. Parashar, and B. B. Tripathi, J. Phys. Chem. Solids **50,** 925 (1989).
[11] H. D. Lutz, W. Becker, B. Müller, and M. Jung, J. Raman Spectrosc. **20,** 99 (1989).
[12] H. D. Lutz, G. Wäschenbach, G. Kliche, and H. Haeuseler, J. Solid State Chem. **48,** 196 (1983).
[13] K. Wakamura, Solid State Commun. **71,** 1033 (1989).
[14] T. Shimanouchi, M. Tsuboi, and T. Miyazawa, J. Chem. Phys. **35,** 1597 (1961).
[15] M. Born and K. Huang, Dynamical Theory of Crystal Lattices, Clarendon, Oxford (1954).
[16] J. R. Hardy, Phil. Mag. **4,** 1278 (1959); J. R. Hardy and A. M. Karo, Phil. Mag. **5,** 859 (1960).
[17] R. J. Hill, J. R. Craig, and G. V. Gibbs, Phys. Chem. Miner. **4,** 317 (1979).
[18] H. D. Lutz, Z. Naturforsch. **24a,** 1417 (1969).
[19] J. Himmrich, Thesis, Univ. Siegen (1990).
[20] A. Yamamoto, T. Utida, H. Murata, and Y. Shiro, J. Phys. Chem. Solids **37,** 693 (1976).
[21] V. Devarajan and W. E. Klee, Phys. Chem. Miner. **7,** 35 (1981).
[22] H. D. Lutz, and M. Fehér, Spectrochim. Acta, Part A, **27,** 357 (1971).
[23] Th. Schmidt and H. D. Lutz, J. Less.-Common Met. (in press).
[24] J. Shanker, G. G. Agrawal, and N. Dutt, Phys. Stat. Sol. B **138,** 9 (1986).
[25] J. Preudhomme and P. Tarte, Spectrochim. Acta, Part A, **27,** 845 (1971).